

STNAGNN: Spatiotemporal Node Attention Graph Neural Network for Task-based fMRI Analysis

Jiyao Wang^{1,*}, Nicha C. Dvornek^{1,2}, Peiyu Duan¹, Lawrence H. Staib^{1,2},
Pamela Ventola⁴, and James S. Duncan^{1,2,3,5}

¹ Biomedical Engineering, Yale University, New Haven, CT 06511, USA

² Radiology & Biomedical Imaging, Yale School of Medicine, New Haven, CT 06511, USA

³ Electrical Engineering, Yale University, New Haven, CT 06511, USA

⁴ Child Study Center, Yale School of Medicine, New Haven, CT, 06511, USA

⁵ Statistics & Data Science, Yale University New Haven, CT, 06511, USA

Abstract. Task-based fMRI uses actions or stimuli to trigger task-specific brain responses and measures them using BOLD contrast. Despite the significant task-induced spatiotemporal brain activation fluctuations, most studies on task-based fMRI ignore the task context information aligned with fMRI and consider task-based fMRI a coherent sequence. In this paper, we show that using the task structures as data-driven guidance is effective for spatiotemporal analysis. We propose STNAGNN, a GNN-based spatiotemporal architecture, and validate its performance in an autism classification task. The trained model is also interpreted for identifying autism-related spatiotemporal brain biomarkers.

Keywords: Graph Neural Network · Autism Spectrum Disorder · fMRI

1 Introduction

A variety of deep learning models including recurrent neural networks (RNNs) [5,2], convolutional neural networks (CNNs) [13], and graph neural networks (GNNs) [16,8,28] are applied to analyzing brain images. Among these studies, many networks are designed for or applied to resting-state functional magnetic resonance imaging (fMRI) [5,8,28]. For those using task-based fMRI data [16,2], the task-based fMRI is analyzed as a coherent sequence similar to resting-state fMRI. However, knowledge of the fMRI task may offer a strong inductive bias for learning an informative model. As such, deep-learning-based analytic methods designed for fMRI analysis with task awareness is underdeveloped.

Compared to resting-state fMRI, task-based fMRI presents more significant blood-oxygen-level-dependent (BOLD) signal fluctuations, especially in its temporal segments acquired under designed task events. It has been shown to be superior to resting-state data for applications like predicting behavioral traits [29]

* Corresponding author: Email: jiyao.wang@yale.edu

and detecting individual differences [11]. Although the diversity of task designs causes considerable difficulties in constructing large task-based fMRI datasets, increasing evidence indicates promising potential value for task-based fMRI.

To utilize task-based fMRI data with both temporal task context and spatial ROI interactions, we formulate our goal as a spatiotemporal graph analysis problem. Specifically, we focus on discrete spatiotemporal graph formation where the spatiotemporal fMRI input is a temporal sequence of “graph snapshots”, where each snapshot corresponds to a sliding window subsequence of the fMRI. Although temporal GNNs are a frequently studied subject in recent years [19,21,1,15,17], we identify two key challenges unique to spatiotemporal brain graph applications:

- From the temporal perspective, the limited temporal resolution of fMRI acquisition and the sliding-window truncation of the sequence data lead to an extremely short sequence of graph snapshots (12 in our experiment), minimizing the advantages of the typical RNN to capture long-term dependencies in temporal information.
- For the spatial graph snapshot of each sliding window, the common correlation-based functional connectome (FC) edge definition is susceptible to noise when applied on short temporal sequences, leading to noisy spatial edges in graph construction. It is even more difficult to define spatiotemporal edges.

To tackle these challenges, we propose STNAGNN, a spatiotemporal GNN model that incorporates a node-level attention algorithm for temporal information aggregation. Instead of defining inaccurate spatiotemporal edges through data engineering, we impose fully-connected spatiotemporal edges on top of spatial graph edges. The proposed pipeline is easily applicable to any task-based fMRI data using block or event-based task schemes.

2 Preliminaries and Model Architectures

2.1 Notation and Problem Definition

We truncate our spatiotemporal fMRI temporally into T subsequences and construct each subsequence into a graph snapshot. For each instance, the input is a sequence of undirected weighted graph snapshots $\{\mathcal{G}_0, \mathcal{G}_1, \dots, \mathcal{G}_{T-1}\}$ where any $\mathcal{G}_i = (\mathcal{V}_i, \mathcal{E}_i)$ is a graph on vertex set \mathcal{V}_i and edge set \mathcal{E}_i . For any edge $(v_{i,j_0}, v_{i,j_1}) \in \mathcal{E}_i$ connecting vertices v_{i,j_0} and v_{i,j_1} , we define its edge weight $e_{i,j_0,j_1} \in \mathbb{R}$ and $e_{i,j_0,j_1} > 0$. For a vertex set of $N_{\mathcal{V}_i}$ vertices, d -dimensional input node features are denoted as $x_{i,j}^0 \in \mathbb{R}^d$ where $j \in \{0, 1, \dots, N_{\mathcal{V}_i} - 1\}$. Based on the above definitions, our goal to perform instance classification is equivalent to learning a mapping function f that maps a sequence of graph snapshots into a class prediction label output Z :

$$f : \{\mathcal{G}_i | i \in \{0, 1, \dots, T-1\}\} \mapsto Z \in \{0, 1\}$$

2.2 Baseline GNN-RNN Model

Intuitively, to analyze spatiotemporal data in the format of sequential graphs, we can combine a GNN with an RNN. We follow this idea to implement our baseline two-step model. As shown in Fig. 1, a two-layer GNN is used to extract graph features from each graph \mathcal{G}_i , followed by an RNN module to aggregate graph embeddings in the temporal sequence.

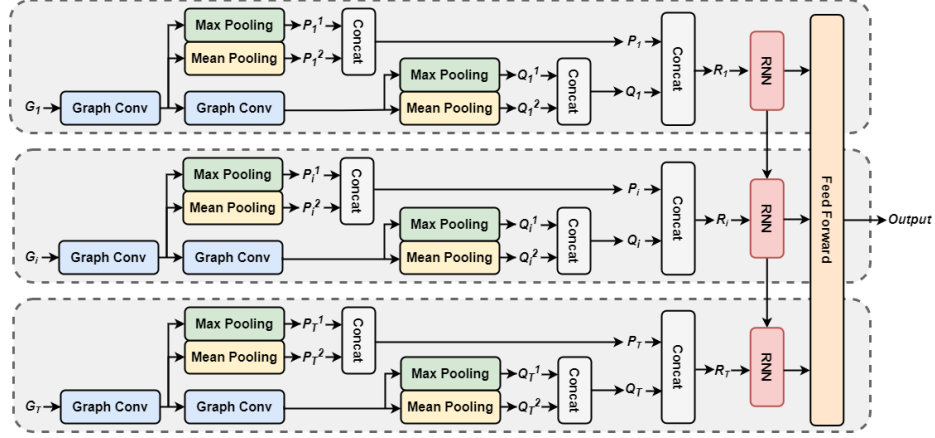


Fig. 1. Baseline GNN-RNN architecture

In this GNN-RNN architecture, spatial aggregation of node features and temporal aggregation of graphs are separated into two steps. The graph convolution blocks aggregate spatial information represented by node features and node-to-node connectivity. Through pooling layers, the node-level information from a graph snapshot is aggregated into a graph-level node-permutation-invariant embedding $\{R_1, R_2, \dots, R_T\}$. In the temporal aggregation step using an RNN, the input embedding has no node-level information.

2.3 STNAGNN Model

In contrast to the GNN-RNN model above, our proposed STNAGNN model maintains node identities in aggregating spatiotemporal information from different graph snapshots. As shown in Fig. 2, after performing two layers of graph convolution, we add positional encoding to each node and compute nodewise self-attention as a spatiotemporal information aggregation operation using the dot product attention algorithm [23]. Essentially, in this operation, we discard the spatial edges defined by FC and impose a fully connected spatiotemporal graph containing all node sets $\{\mathcal{V}_0, \mathcal{V}_1, \dots, \mathcal{V}_{T-1}\}$ from a sequence of graph snapshots.

In both the Transformer [23] and Vision Transformer [4], additive positional encoding for dot product attention is a 1-dimensional raster sequence sine and

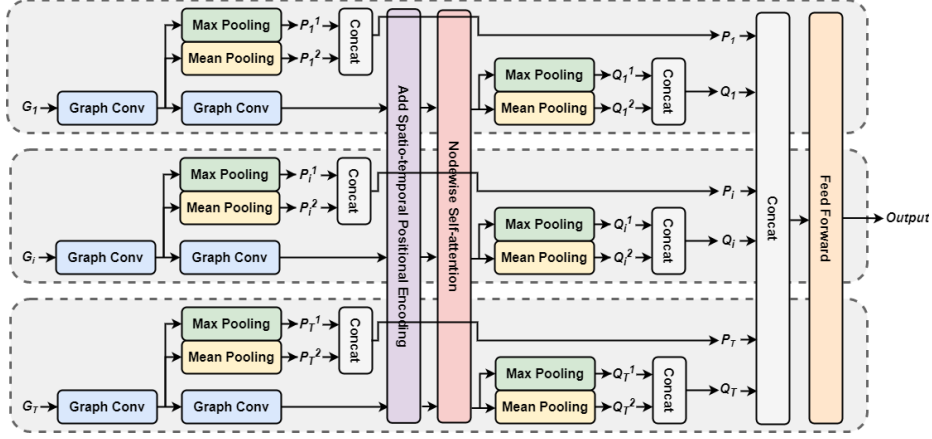


Fig. 2. STNAGNN architecture

cosine function. In our spatiotemporal application, to encode both spatial and temporal information of a node, we add a 2-dimensional positional encoding defined as follows:

$$PE(j, i, 2f) = \sin(j/10000^{2f/d_{model}}) \sin((10000 + i)/10000^{2f/d_{model}}) \quad (1)$$

$$PE(j, i, 2f + 1) = \cos(j/10000^{2f/d_{model}}) \cos((10000 + i)/10000^{2f/d_{model}}) \quad (2)$$

where j denotes spatial position and i denotes temporal position. f represents the individual feature channel among node features of dimension d_{model} .

We argue that there are several advantages in applying the spatiotemporal self-attention operation in the STNAGNN architecture:

- By using a fully-connected self-attention operation, we avoid the bias from noisy edge definition. Information aggregation becomes data-driven, relying on the updated node features and the spatiotemporal adjacency of nodes.
- A fully connected graph allows for direct participation of information from one node to any other nodes (Fig. 3). It alleviates the problem of limited receptive fields in common graph convolution operations [14,24].
- Similar to the scenario in the Transformer [23], all graph convolutions can now be computed in parallel. It is more efficient than the sequential computation in RNN-based temporal GNN architectures [21,15,17].

3 Data and Preprocessing

We use a 118-subject task-based fMRI dataset to test our model under an autism spectrum disorder (ASD) classification task. It contains fMRI scans of 75 ASD children and 43 age-and-IQ-matched healthy controls. The scans are acquired

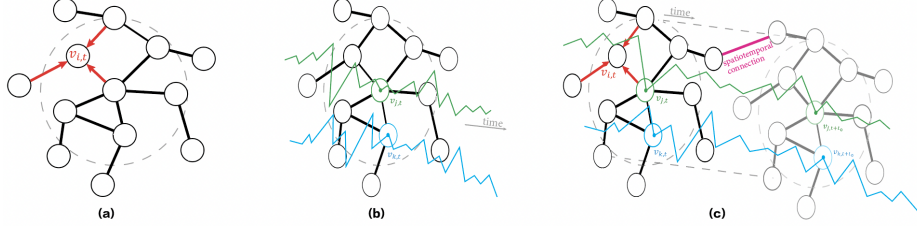


Fig. 3. Illustration of connectivity types: a) spatial connectivity; b) temporal connectivity; c) spatiotemporal connectivity (magenta). Existing architectures usually consider only spatial connectivity [16] or temporal connectivity [5]. Some spatiotemporal designs consider both spatial and temporal perspectives [8] but use a two-step spatial-then-temporal approach. Our STNAGNN jointly considers spatial, temporal, and spatiotemporal connectivity.

under the “biopoint” [12] task containing 12 videos of either biological or scrambled motions of point light displays. Videos from these two categories are given to subjects in alternating sequence during the scan with an intention to highlight deficits in motion perception in autistic children.

The scan for each subject has 146 frames with a frame rate of 2 seconds and a voxel size of $3.2mm \times 3.2mm \times 3.2mm$. It is collected at Yale Child Study Center, approved by Yale University Institutional Review Board. Acquired fMRI data is preprocessed using a pipeline [26] including steps of motion correction, interleaved slice timing correction, BET brain extraction, grand mean intensity normalization, spatial smoothing, and high-pass temporal filtering.

4 Graph Construction and Training

As shown in Fig. 4, we first parcellate the brain fMRI data into 84 ROIs based on the Desikan-Killiany atlas [3]. Then, the mean time series of each ROI is extracted using 1/3 of all voxels by bootstrap random sampling [6]. For network training, we performed stratified sampling of the 118 subjects with roughly 80%/20% split of training/testing set, and sample each ROI 30 times as augmentation, resulting in 2820/720 instances.

For our “biopoint” dataset, we truncate the mean time series into 12 subsequences aligned with each video stimuli. This task-structure-based truncation is verified to be produce better performance than sliding window approach in previous experiments using another GNN architecture [16]. For each local subsequence time series, we calculate FC between ROIs and use it as node features. Meanwhile, we extract and concatenate all the times series acquired under biological motion videos. Using the concatenated sequence, we calculate a global biological FC and use its top 5% values to define edges and their weights for graph sparsity. Edges are shared across all 12 graph snapshots of each instance. We have previously observed empirically that for a different GNN model run on

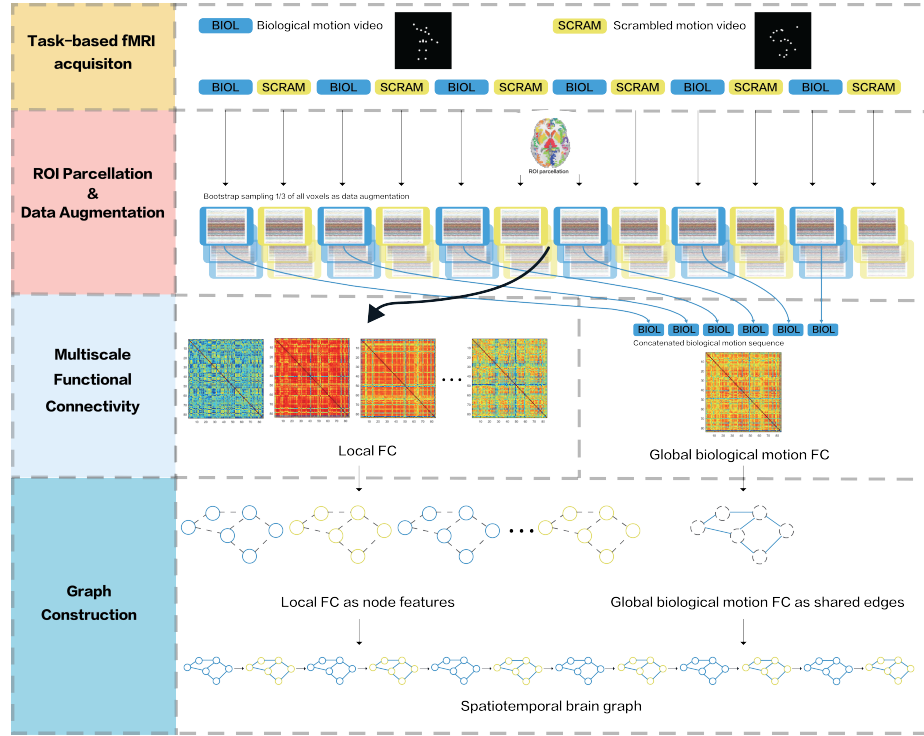


Fig. 4. Preprocessing and graph construction pipeline

biopoint data, assigning edges using the global biological FC improves performance compared to the whole sequence or global scrambled FC. As the biological motion viewing task is expected to elicit stronger correlated activity than the more random scrambled motion viewing task, we choose to use the global biological FC for all edges.

During training, we experiment with alternative two-layered graph convolution operations and temporal aggregation methods. In the MLP modules following graph convolution and temporal aggregation methods, we apply SiLU [7] activation and a dropout rate of 0.2 in each layer. All models are trained with binary cross-entropy loss on a RTX 2080 Ti GPU.

$$Loss = -(y \log(p) + (1 - y) \log(1 - p)) \quad (3)$$

5 Evaluation and Interpretation

5.1 Classification Performance

For the baseline GNN-RNN architecture, we experiment with alternatives in GNN layers and RNN modules on the ASD classification task. Model performance is summarized in Table 1.

Table 1. Baseline GNN-RNN Performance on ASD Classification

Method	LSTM[10]			Bidirectional LSTM		
	Accuracy(%)	F1	AUC	Accuracy(%)	F1	AUC
GCN[14]	61.1	0.652	0.620	62.6	0.668	0.634
GAT[24]	70.0	0.771	0.664	71.8	0.780	0.691
GraphSAGE[9]	71.0	0.760	0.701	72.4	0.790	0.687
GIN[25]	65.6	0.722	0.636	66.5	0.675	0.702
GraphTransformer[22]	69.9	0.767	0.667	70.7	0.757	0.699

For the proposed STNAGNN architecture, we first empirically show for two different GNN baselines that using the proposed 2-dimensional encoding improves model performance on the ASD classification task compared to using 1-dimensional raster sequence positional encoding (Table 2).

Table 2. ASD Classification Performance of STNAGNN using GCN and GAT with 1D/2D Positional Encoding

Method	1D Raster Sequence PE			2D Spatiotemporal PE		
	Accuracy(%)	F1	AUC	Accuracy(%)	F1	AUC
GCN[14]	74.6	0.819	0.687	75.7	0.828	0.698
GAT[24]	78.9	0.854	0.721	82.4	0.872	0.777

Additionally, we experiment with 2-dimensional positional encoding and alternatives in GNN layers for the ASD classification task. The performance is compared with existing temporal GNN architectures in Table 3.

Table 3. ASD Classification Performance of Temporal GNN Models and STNAGNN with GNN Design Alternatives

Method		Accuracy(%)	F1	AUC
Temporal GNN	GConvGRU[21]	67.1	0.752	0.629
	GConvLSTM[21]	67.9	0.759	0.637
	GCLSTM[1]	72.6	0.802	0.674
	LRGCN[15]	66.5	0.749	0.621
	EvolveGCN[17]	75.8	0.819	0.720
	STGCN[8]	69.9	0.795	0.620
STNAGNN	GCN[14]	75.7	0.828	0.698
	GAT[24]	82.4	0.872	0.777
	GraphSAGE[9]	72.2	0.815	0.636
	GIN[25]	71.3	0.800	0.644
	GraphTransformer[22]	71.0	0.801	0.634

From the above results, the proposed STNAGNN architecture with GAT and 2D positional encoding has the best performance across all metrics. It outperforms all design alternatives under the GNN-RNN architecture and compared state-of-the-art temporal GNNs designed for discrete graph snapshots.

5.2 Biomarker Identification

To interpret the trained STNAGNN model, we apply the GNNExplainer[27], designed as a post-hoc interpretability method. We consider all the $1008 = 84 \times 12$ spatiotemporal nodes and derive an importance score for each node by optimizing towards highest mutual information with masked input nodes. The heatmap for node importance scores are shown in Fig. 5 with the temporal sequence marked in the top-left corner of each plot. Darker ROIs have higher importance to the final classification output.

In individual heatmaps, we observe structures such as the frontal gyrus and thalamus recurring as regions more important than the surroundings. While the thalamus is considered highly associated with ASD [20], the frontal gyrus is also connected with functions including emotion, attention, and decision-making [18], which are important metrics for ASD. Across all heatmaps, we do not observe obvious regions being important in all graph snapshots, which is potentially evidence for dynamic functional communities across temporal space.

6 Conclusion

Task-based fMRI is long considered less practical than resting-state fMRI in a deep learning setting due to the difficulty in acquiring a large dataset and its

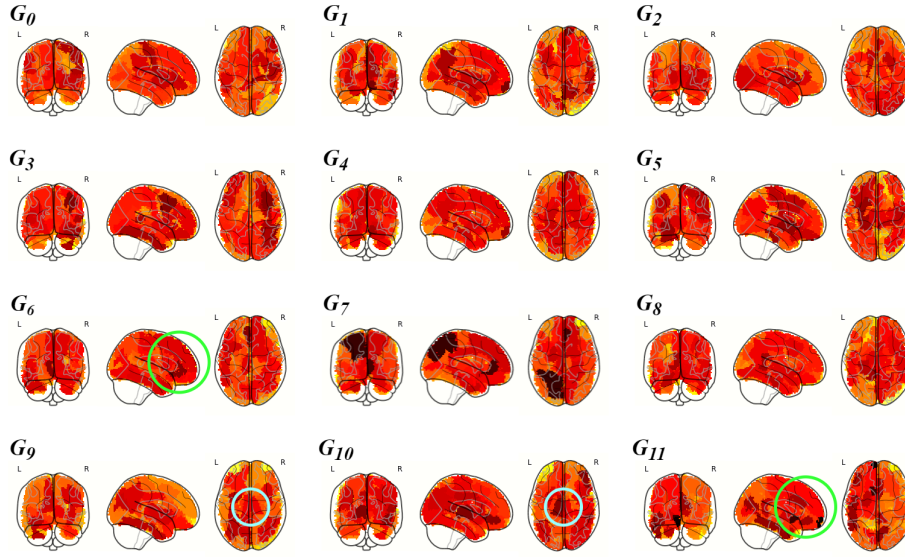


Fig. 5. Heatmaps for spatiotemporal ROI importance scores. Darker color indicates higher importance. Green circles show two instances of frontal gyrus. Blue circles show two instances of thalamus.

limited performance gain when trained as a coherent sequence. By spatiotemporal task-aware modeling, we show the promising potential of task-based fMRI in analyzing brain dynamics. In future research, besides expanding the experiments to more datasets, we intend to explore more flexibility in spatiotemporal brain graph modeling including dynamic edges and dynamic ROI parcellation.

References

1. Chen, J., Xu, X., Wu, Y., Zheng, H.: GC-LSTM: graph convolution embedded LSTM for dynamic link prediction. CoRR **abs/1812.04206** (2018)
2. Dakka, J., Bashivan, P., Gheiratmand, M., Rish, I., Jha, S., Greiner, R.: Learning neural markers of schizophrenia disorder using recurrent neural networks. CoRR **abs/1712.00512** (2017)
3. Desikan, R.S., Ségonne, F., Fischl, B., Quinn, B.T., Dickerson, B.C., Blacker, D., Buckner, R.L., Dale, A.M., Maguire, R.P., Hyman, B.T., Albert, M.S., Killiany, R.J.: An automated labeling system for subdividing the human cerebral cortex on mri scans into gyral based regions of interest. NeuroImage **31**(3), 968–980 (2006). <https://doi.org/https://doi.org/10.1016/j.neuroimage.2006.01.021>
4. Dosovitskiy, A., Beyer, L., Kolesnikov, A., Weissenborn, D., Zhai, X., Unterthiner, T., Dehghani, M., Minderer, M., Heigold, G., Gelly, S., Uszkoreit, J., Houshy, N.: An image is worth 16x16 words: Transformers for image recognition at scale. CoRR **abs/2010.11929** (2020)

5. Dvornek, N., Ventola, P., Pelphrey, K., Duncan, J.: Identifying autism from resting-state fmri using long short-term memory networks. In: Machine learning in medical imaging. MLMI (Workshop). vol. 10541, pp. 362–370 (09 2017). https://doi.org/10.1007/978-3-319-67389-9_42
6. Dvornek, N.C., Yang, D., Ventola, P., Duncan, J.S.: Learning generalizable recurrent neural networks from small task-fmri datasets. In: International Conference on Medical Image Computing and Computer-Assisted Intervention. pp. 329–337. Springer (2018)
7. Elfving, S., Uchibe, E., Doya, K.: Sigmoid-weighted linear units for neural network function approximation in reinforcement learning. CoRR **abs/1702.03118** (2017)
8. Gadgil, S., Zhao, Q., Pfefferbaum, A., Sullivan, E.V., Adeli, E., Pohl, K.M.: Spatio-temporal graph convolution for resting-state fmri analysis. Medical image computing and computer-assisted intervention : MICCAI ... International Conference on Medical Image Computing and Computer-Assisted Intervention **12267**, 528–538 (2020)
9. Hamilton, W.L., Ying, R., Leskovec, J.: Inductive representation learning on large graphs. CoRR **abs/1706.02216** (2017)
10. Hochreiter, S., Schmidhuber, J.: Long short-term memory. Neural computation **9**, 1735–80 (12 1997). <https://doi.org/10.1162/neco.1997.9.8.1735>
11. Jiang, R., Zuo, N., Ford, J.M., Qi, S., Zhi, D., Zhuo, C., Xu, Y., Fu, Z., Bustillo, J., Turner, J.A., Calhoun, V.D., Sui, J.: Task-induced brain connectivity promotes the detection of individual differences in brain-behavior relationships. NeuroImage **207**, 116370 (2020). <https://doi.org/https://doi.org/10.1016/j.neuroimage.2019.116370>
12. Kaiser, M.D., Hudac, C.M., Shultz, S., Lee, S.M., Cheung, C., Berken, A.M., Deen, B., Pitskel, N.B., Sugrue, D.R., Voos, A.C., Saulnier, C.A., Ventola, P., Wolf, J.M., Klin, A., Wyk, B.C.V., Pelphrey, K.A.: Neural signatures of autism. Proceedings of the National Academy of Sciences **107**(49), 21223–21228 (2010). <https://doi.org/10.1073/pnas.1010412107>
13. Kawahara, J., Brown, C.J., Miller, S.P., Booth, B.G., Chau, V., Grunau, R.E., Zwicker, J.G., Hamarneh, G.: Brainnetcnn: Convolutional neural networks for brain networks; towards predicting neurodevelopment. NeuroImage **146**, 1038–1049 (2017). <https://doi.org/https://doi.org/10.1016/j.neuroimage.2016.09.046>
14. Kipf, T.N., Welling, M.: Semi-supervised classification with graph convolutional networks. CoRR **abs/1609.02907** (2016)
15. Li, J., Han, Z., Cheng, H., Su, J., Wang, P., Zhang, J., Pan, L.: Predicting path failure in time-evolving graphs. CoRR **abs/1905.03994** (2019)
16. Li, X., Zhou, Y., Dvornek, N., Zhang, M., Gao, S., Zhuang, J., Scheinost, D., Staib, L.H., Ventola, P., Duncan, J.S.: Braingnn: Interpretable brain graph neural network for fmri analysis. Medical Image Analysis **74**, 102233 (2021). <https://doi.org/https://doi.org/10.1016/j.media.2021.102233>
17. Pareja, A., Domeniconi, G., Chen, J., Ma, T., Suzumura, T., Kanezashi, H., Kaler, T., Leiserson, C.E.: Evolvegcnn: Evolving graph convolutional networks for dynamic graphs. CoRR **abs/1902.10191** (2019)
18. Press, C., Weiskopf, N., Kilner, J.M.: Dissociable roles of human inferior frontal gyrus during action execution and observation. NeuroImage **60**(3), 1671–1677 (2012). <https://doi.org/https://doi.org/10.1016/j.neuroimage.2012.01.118>
19. Rossi, E., Chamberlain, B., Frasca, F., Eynard, D., Monti, F., Bronstein, M.M.: Temporal graph networks for deep learning on dynamic graphs. CoRR **abs/2006.10637** (2020)

20. Schuetze, M., Park, M.T.M., Cho, I.Y., MacMaster, F.P., Chakravarty, M., Bray, S.L.: Morphological alterations in the thalamus, striatum, and pallidum in autism spectrum disorder. *Neuropsychopharmacology* **41**, 2627 – 2637 (2016)
21. Seo, Y., Defferrard, M., Vandergheynst, P., Bresson, X.: Structured sequence modeling with graph convolutional recurrent networks. In: *Neural Information Processing: 25th International Conference, ICONIP 2018, Siem Reap, Cambodia, December 13-16, 2018, Proceedings, Part I* 25. pp. 362–373. Springer (2018)
22. Shi, Y., Huang, Z., Wang, W., Zhong, H., Feng, S., Sun, Y.: Masked label prediction: Unified message passing model for semi-supervised classification. *CoRR* **abs/2009.03509** (2020)
23. Vaswani, A., Shazeer, N., Parmar, N., Uszkoreit, J., Jones, L., Gomez, A.N., Kaiser, L., Polosukhin, I.: Attention is all you need (2017). <https://doi.org/10.48550/ARXIV.1706.03762>
24. Veličković, P., Cucurull, G., Casanova, A., Romero, A., Liò, P., Bengio, Y.: Graph attention networks. In: *International Conference on Learning Representations* (2018)
25. Xu, K., Hu, W., Leskovec, J., Jegelka, S.: How powerful are graph neural networks? *CoRR* **abs/1810.00826** (2018)
26. Yang, D., Pelphrey, K.A., Sukhodolsky, D.G., Crowley, M.J., Dayan, E., Dvornek, N.C., Venkataraman, A., Duncan, J., Staib, L., Ventola, P., et al.: Brain responses to biological motion predict treatment outcome in young children with autism. *Translational Psychiatry* **6**(11) (2016). <https://doi.org/10.1038/tp.2016.213>
27. Ying, R., Bourgeois, D., You, J., Zitnik, M., Leskovec, J.: GNN explainer: A tool for post-hoc explanation of graph neural networks. *CoRR* **abs/1903.03894** (2019)
28. Zhang, H., Song, R., Wang, L., Zhang, L., Wang, D., Wang, C., Zhang, W.: Classification of brain disorders in rs-fmri via local-to-global graph neural networks. *IEEE Transactions on Medical Imaging* **42**(2), 444–455 (2023). <https://doi.org/10.1109/TMI.2022.3219260>
29. Zhao, W., Makowski, C., Hagler, D.J., Garavan, H.P., Thompson, W.K., Greene, D.J., Jernigan, T.L., Dale, A.M.: Task fmri paradigms may capture more behaviorally relevant information than resting-state functional connectivity. *NeuroImage* **270**, 119946 (2023). <https://doi.org/https://doi.org/10.1016/j.neuroimage.2023.119946>